Geochemistry and Mineralogy of Ilmenite Exsolutions in Titanomagnetite and Their Implications for the Ore-Forming Process at the Damiao Deposit.

Kaiyuan Wang[a,*], Hongtao He[a], Wenjie Shi[a]
[a] *School of Earth Science and Engineering, Hebei University of Engineering, Handan 056038, Hebei, China*

* Corresponding author at: School of Earth Science and Engineering, Hebei University of Engineering, Taiji Road, Handan 056038, China.
E-mail address: wangkaiyuan@hebeu.edu.cn

This paper is a postprint submitted to EarthArXiv. The paper has been peer-reviewed and accepted for publication in the journal Acta Geochimica.

Geochemistry and Mineralogy of Ilmenite Exsolutions in Titanomagnetite and Their Implications for the Ore-Forming Process at the Damiao Deposit

Abstract:

The Damiao Fe-Ti-P deposit, located within the Damiao anorthosite complex in northeastern China, features Fe-Ti oxide ores and nelsonites occurring as irregularly inclined stratiform-like bodies, lenses, or veins with sharp contacts against anorthosite and gabbronorite. The deposit is characterized by abundant titanomagnetite hosting diverse ilmenite exsolution textures, including blocky, lamellar, and cloth-like forms. In this study, we investigate the geochemistry and mineralogy of ilmenite exsolutions in titanomagnetite to understand their formation mechanisms and implications for the ore-forming process. Detailed petrographic observations and electron microprobe analyses reveal that the exsolution textures result from multiple mechanisms: oxy-exsolution due to oxidation of titanomagnetite; subsolidus re-equilibration between magnetite and ilmenite involving elemental diffusion of Fe, Ti, Cr, Co, and Ni; and exsolution related to lattice defects caused by rapid cooling. Thermodynamic modeling using Gibbs free energy calculations and the QUILF program indicates that blocky, lamellar, and cloth-textured ilmenite exsolutions formed at temperatures both above and below the solid solution solvus under different oxygen fugacities. These findings suggest that multiple oxidation events of a compositionally homogeneous Fe-Ti-P magma under varying thermal conditions led to the observed diversity of ilmenite exsolution textures. Additionally, our results indicate that the exsolution of

zircon at ilmenite grain boundaries is attributed to interactions between ilmenite and adjacent clinopyroxene. The formation of hercynite is linked to increased aluminum content in the solid solution due to the oxidation exsolution of ilmenite. Reconstruction of the cooling history suggests that the iron-titanium oxide ores crystallized from a ferrodioritic magma. Increasing oxygen fugacity during magma evolution promoted immiscibility, leading to the formation of Fe-Ti-P-rich melts and ultimately the development of nelsonitic ores.

Key words: Ilmenite exsolution; Oxy-exsolution; Titanomagnetite; Subsolidus re-equilibration; Damiao Fe-Ti-P deposit

1. Introduction

Magmatic Fe-Ti oxide deposits are significant sources of iron, titanium, vanadium, and phosphorus, commonly associated with mafic-ultramafic intrusions and Proterozoic anorthosite complexes (Pang et al., 2010; She et al., 2014; Charlier et al., 2015). The Damiao deposit is a prominent example characterized by abundant titanomagnetite hosting complex ilmenite exsolution textures (Wei et al., 2020; Li et al., 2019). Understanding the formation mechanisms of these exsolutions is crucial for unraveling the ore-forming processes and the thermal history of the deposit.

Titanomagnetite, as solid solution of magnetite (Fe_3O_4) and ulvöspinel (Fe_2TiO_4), crystallizes from Fe-Ti-rich magmas under varying temperature and oxygen fugacity conditions (Arguin et al., 2018; Tan et al., 2016). Upon cooling, titanomagnetite often undergoes subsolidus exsolution, resulting in the precipitation of ilmenite ($FeTiO_3$) and other oxide phases. The textures and compositions of these exsolved minerals

provide valuable insights into the physicochemical conditions during and after crystallization (Price, 1981; Gruenewaldt et al., 1985; Harrison and Putnis, 1997; Gao et al., 2019).

Several mechanisms have been proposed for the formation of ilmenite exsolutions in titanomagnetite, including oxy-exsolution due to the oxidation of the ulvöspinel component at high temperatures, subsolidus re-equilibration between magnetite and ilmenite during cooling, and cation-deficient mechanisms associated with rapid cooling and lattice defects (Frost, 1991; Tan et al., 2016; Gao et al., 2019; Arguin et al., 2018). Despite extensive studies, the precise mechanisms responsible for ilmenite exsolution and their relative contributions remain subjects of debate. Moreover, the role of factors such as oxygen fugacity, cooling rates, and magma composition in controlling these processes is not fully understood.

In the Damiao deposit, previous research has documented the presence of various ilmenite exsolution textures within titanomagnetite, including blocky, lamellar, and cloth-like structures (Wei et al., 2020; Li et al., 2019). However, a comprehensive geochemical and mineralogical analysis of these exsolutions is lacking. Such an investigation is important for interpreting the cooling history of the Fe-Ti-P oxide rocks and assessing the implications for the ore-forming processes.

In this study, we examine the geochemistry and mineralogy of ilmenite exsolutions in titanomagnetite from the Damiao deposit. By analyzing the compositions and textures of these exsolutions, we aim to better understand their formation mechanisms and the conditions under which they formed. Additionally, we

discuss the implications of our findings for the cooling history of the Damiao Fe-Ti-P oxide rocks and the ore-forming processes involved.

2. Geological Background

The North China Craton, a significant Archean to Paleoproterozoic geological entity, was formed through the amalgamation of the Eastern and Western Blocks along the Trans-North China Orogen (TNCO) around 1.85 Ga (Yan et al., 2025; Wan et al., 2013. Fig.1). This orogenic belt served as the suture zone where the two blocks collided and stabilized to create the craton. The basement rocks of the craton consist predominantly of high-grade metamorphic assemblages, including granitic migmatites, gneisses, schists, and marbles, overlain by Mesoproterozoic to Cenozoic sedimentary sequences (Li et al., 2024; He et al., 2016).

Located in the northern part of the TNCO, the Damiao anorthosite complex is a prominent Proterozoic intrusion emplaced approximately 1.74 Ga during a post-collisional tectonic setting (Chen et al., 2013; He et al., 2016. Fig.1). This complex is a key component of the Anorthosite–Mangerite–Charnockite–Granite (AMCG) suite, which is temporally and spatially associated with rapakivi granites and reflects significant crustal differentiation events during the late Paleoproterozoic (Yang et al., 2014; Liu et al., 2016). The Damiao complex intruded into Neoarchean high-grade metamorphic rocks of the Dantazi Group, dated at around 2.5 Ga, and is unconformably overlain by Jurassic volcanic and sedimentary rocks (Li et al., 2019; Zhai and Santosh, 2013).

The Damiao anorthosite complex is divided into three distinct bodies: the

Eastern, Central, and Western Bodies (Zhao et al., 2009; Li et al., 2019. Fig.1). The Western Body, being the largest with an area of approximately 80 km^2, comprises extensive volumes of anorthosite along with minor occurrences of leuconorite, oxide–apatite gabbronorite, mangerite, and significant Fe–Ti–P orebodies (He et al., 2016, 2019; Zhao et al., 2009). Deep drilling beneath the Western Body has revealed a substantial olivine–titanomagnetite-rich layered intrusion, suggesting the presence of mafic residues from the differentiation of a high-aluminum basaltic parental magma (He et al., 2016, 2019; Zhao et al., 2009).

Magmatic activity within the Damiao complex is characterized by two main stages. The early stage involved the emplacement of anorthosite with minor norite components, while the late stage introduced mangerite and Fe–Ti–P-rich dikes and veins that intruded the existing anorthosite massif (Wang et al., 2017; Li et al., 2014, 2019). The early-stage anorthosite exhibits two facies based on coloration: a dark-colored, relatively unaltered variety, and a light-colored, extensively altered type (Wei et al., 2020). The dark-colored anorthosite primarily consists of plagioclase ($An_{40–55}$) and subordinate amounts of pyroxenes (hypersthene and diopside) and Fe–Ti oxides. In contrast, the light-colored anorthosite has undergone hydrothermal alteration, with plagioclase transformed into albite and clinozoisite and pyroxenes replaced by chlorite and magnetite (Teng et al., 2015; Li et al., 2014, 2019).

Fe–Ti–P-rich rocks in the Damiao complex occur as dikes and veins with irregular yet sharp contacts, crosscutting the earlier anorthosite units. These rocks include oxide–apatite gabbronorite, Fe–Ti–P-rich pyroxenite, and massive Fe–Ti–(P)

orebodies (Chen et al., 2013; He et al., 2016; 2019. Fig.1). The orebodies are predominantly lens-shaped or form steeply inclined stratiform bodies within the anorthosite and leuconorite, displaying various sizes that can reach up to tens of meters in width and hundreds of meters in length. Mineralogical zoning within these orebodies is common, with apatite-rich zones near the tops and margins and oxide-rich zones toward the centers and bases, indicating possible gravitational differentiation during crystallization (Zhao et al., 2009; Li et al., 2014, 2019).

The complex also hosts minor occurrences of mangerite, particularly in the northwestern region of the Western Body, which is considered a late-stage differentiative product of the parental magma. Additionally, ferrodioritic, gabbroic, and felsic dykes are present, suggesting multiple intrusive events and a prolonged magmatic history (Chen et al., 2013; He et al., 2016; 2019).

3. Analytical methods

3.1. Whole-Rock Major Element Analysis:

Bulk rock samples were crushed and pulverized to a fine powder for whole-rock geochemical analysis. Major elements were determined by X-ray fluorescence (XRF) spectrometry using a Rigaku ZSX Primus II XRF instrument at the ALS Laboratory Group. Fused glass beads were prepared from the powdered samples using a lithium tetraborate flux. Calibration was performed using certified reference materials GSR-1 to GSR-6 issued by the Chinese National Standards. Analytical precision and accuracy were monitored by repeated analyses of standard reference materials and duplicates, with relative standard deviations better than 2% for most major elements.

Trace element geochemistry was analyzed by ICP – MS at the Institute of Geochemistry, Guiyang (Chinese Academy of Sciences, GIGCAS). Detailed analytical methodology was outlined in Qi and Zhou (2008).

3.2. Electron Probe Microanalysis (EPMA):

Mineral compositions of magnetite, ilmenite, clinopyroxene, and apatite were determined using a JEOL JXA-8230 electron probe microanalyzer (EPMA) at the GIGCAS. Backscattered electron (BSE) imaging was employed to identify exsolution textures and select suitable areas for analysis. The analytical conditions were optimized to obtain accurate major element concentrations: an accelerating voltage of 15 kV, a beam current of 20 nA, and a focused beam diameter of 1 μm. Natural and synthetic standards were used for calibration, including Fe_2O_3 for iron, TiO_2 for titanium, Cr_2O_3 for chromium, $MnTiO_3$ for manganese, and NiO for nickel. Matrix corrections were applied using the ZAF method. Detection limits for most elements were below 0.01 wt%. To avoid beam damage and element migration, particularly for alkali elements in apatite, a defocused beam (5 μm) was used when necessary.

3.3. Laser Ablation Inductively Coupled Plasma Mass Spectrometry

Trace element concentrations in magnetite, ilmenite, plagioclase, and apatite were measured by LA-ICP-MS at the GIGCAS. An Agilent 7900 ICP-MS instrument was coupled with a resolution SE 193 nm ArF excimer laser ablation system equipped with a two-volume S-155 ablation cell (Australian Scientific Instruments). The laser spot sizes were 44 μm for apatite and plagioclase, and 60 μm for magnetite and ilmenite, with a repetition rate of 6 Hz and energy density of ~3.5 J/cm^2. Helium was

used as the carrier gas to transport the ablated aerosol to the ICP-MS, with argon make-up gas introduced before the plasma. Calibration was performed using NIST SRM 610 as the external standard and ^{57}Fe or ^{43}Ca as internal standards for magnetite/ilmenite and apatite/plagioclase, respectively. Repetition of analyses on standard reference materials BCR-2G, BHVO-2G, and BIR-1G served to monitor accuracy and precision, yielding results within 5% of recommended values. Data reduction was carried out using the software Iolite, following the protocols described by Paton et al. (2011). Special attention was given to exclude inclusions and surface contamination by examining time-resolved spectra; signals with irregularities were discarded. Detection limits for trace elements were typically in the range of 0.01 to 0.1 ppm.

4. Results

4. 1. Mineral Chemistry of Magnetite, Ilmenite, and Hercynite

The magnetite in the Damiao Fe-Ti-P deposit exhibits a relatively narrow range of compositions. Most magnetite samples have Fe_3O_4 content exceeding 90%, with TiO_2 and Al_2O_3 contents both below 1%. Trace elements in magnetite show a wide range of variability, with higher concentrations of siderophile elements such as Cr, Co, Ni, Ti, and Zn. The positive correlations between FeO and TiO_2, Al_2O_3 indicate that these elements are incorporated into the crystal lattices of magnetite and ilmenite during crystallization (Fig. 6).

Granular ilmenite exhibits Fe_2O_3 contents ranging from 5% to 25%, with almost no pure $FeTiO_3$ present. MnO content fluctuates around 1%. In addition to Fe and Ti,

ilmenite contains significant trace elements, with relatively high concentrations of Zn and V. The composition of exsolved ilmenite lamellae in titanomagnetite is similar to that of granular ilmenite. Hercynite is mainly distributed at the interface between magnetite and exsolved ilmenite, with primary components including Al_2O_3, FeO, and TiO_2 (Fig. 6).

4. 2. Exsolution Textures in Titanomagnetite

The exsolution textures of ilmenite in titanomagnetite show diversity, indicating complex thermal histories and crystallization processes. They can be primarily categorized into three types: blocky, lamellar, and cloth-like.

Blocky Exsolutions: Blocky exsolutions of ilmenite mainly appear as thick lamellae aligned along multiple {111} planes of the magnetite crystal lattice, forming a grid-like pattern. These lamellae, tens to hundreds of microns thick, indicate formation under high-temperature conditions. Blocky exsolutions are typically observed in the core areas of titanomagnetite grains, reflecting the initial high-temperature exsolution process (Fig. 3).

Lamellar Exsolutions: Lamellar exsolutions of ilmenite are predominantly aligned along a single set of {111} planes, usually with a thickness exceeding 100 microns. This texture suggests significant growth under prolonged high-temperature conditions, indicating that ilmenite underwent an exsolution process during high-temperature conditions (Fig. 5).

Cloth-Like Exsolutions: Cloth-like exsolutions primarily include fabric-like textures, thin lamellae, and mottled vermicular intergrowths. Fabric-like textures are

characterized by minute ilmenite intergrowths dispersed throughout the magnetite matrix, resembling woven fabric patterns, indicative of the initial oxidation stage of titanomagnetite at lower temperatures. Thin lamellae are aligned along {111} planes with a thickness ranging from 1 to 5 microns. Mottled and vermicular intergrowths typically occur near grain boundaries and fractures, varying in size from a few microns to several tens of microns, indicating advanced stages of ilmenite exsolution during diffusion (Fig. 5).

Additionally, there are exsolutions of hercynite and zircon within ilmenite. Zircon exsolutions are primarily distributed at grain boundaries as minute inclusions. These zircon inclusions are typically aligned along fractures or interfaces between ilmenite and other minerals, such as clinopyroxene (Fig. 4).

5. Disscussion

5.1. Formation of Ilmenite Exsolution Textures in Magnetite-Ulvöspinel Solid Solution

In iron-rich, titanium-phosphorus magmas, the crystallization of minerals such as magnetite, ilmenite, apatite, and rutile reflects the evolution of magma temperature, oxygen fugacity, and composition (Bhattacharjee and Mondal, 2021; Tan et al., 2016, 2021). Currently, three potential mechanisms have been proposed for the formation of exsolved ilmenite: oxy-exsolution of titanomagnetite; inter-oxide re-equilibration between magnetite and ilmenite; the formation of ilmenite due to cation deficiency caused by rapid cooling of magma leading to lattice defects (Arguin et al., 2018; Wei et al., 2020). Magnetite-ulvöspinel solid solutions can transform into ilmenite under

oxidizing conditions, and the composition and structure of the resulting ilmenite vary depending on temperature, oxygen fugacity, and the composition of the solid solution (Lusted, 2019; Gorbatova et al., 2021). Therefore, the blocky, lamellar, and cloth-textured ilmenite exsolutions observed in the Damiao magnetite deposit are likely formed during different stages of Fe-Ti-P magmatic evolution (Fig. 4, 6). The solvus temperature of magnetite-ulvöspinel solid solutions fluctuates with changes in chemical composition, peaking at approximately 450–600 °C (Otto, 2017; Arguin et al., 2018). The similar spatial distribution and chemical composition among the various structural types of ilmenite exsolutions in the Damiao deposit suggest that the structural diversity is primarily the result of multiple oxidation reactions occurring in compositionally uniform Fe-Ti-P magma under varying temperature conditions (Fig. 4, 6). Temperature and oxygen fugacity calculations for magnetite-ilmenite pairs also indicate that blocky and lamellar ilmenite exsolutions formed above the solvus temperature, whereas cloth-textured ilmenite exsolutions formed below the solvus temperature. Alternatively, multiple magma injections leading to compositional heterogeneity could have resulted in the formation of ilmenite exsolutions with different structural types in various parts of the magma chamber under lower temperature conditions (Lee et al., 2022; Khedr et al., 2024).

$$6Fe_2TiO_4 + O_2 = 6FeTiO_3 + 2Fe_3O_4 \quad (1)$$

Experimental studies have demonstrated that magnetite-ulvöspinel solid solutions can produce various types of ilmenite exsolutions through vacancy relaxation mechanisms under high temperatures (>900 °C) and anoxic reducing

conditions (Pearce et al., 2010; Lilova et al., 2012). In this process, Fe^{2+} ions replace high-valence ions such as Ti^{4+} and Cr^{3+} in adjacent ilmenite, leading to lattice defects (Noh et al., 2015; Özdemir and Dunlop, 1997). This mechanism effectively explains the exsolution textures of iron-titanium oxides in mantle xenoliths (Lattard, 1995). However, as magma temperature decreases and oxygen fugacity increases, the probability of lattice defect formation decreases significantly (Lattard, 1995). Therefore, this mechanism cannot be considered the primary cause of ilmenite exsolution textures in igneous or metamorphic rocks. Based on subsolidus re-equilibration reactions between magnetite and ilmenite, as well as the oxidation reactions of titanomagnetite, the formation temperature of ilmenite exsolution textures in Damiao depsoit is approximately 550–680 °, These conditions do not align with those required for lattice defect–induced ilmenite exsolution.

Both the oxidation of titanomagnetite and the re-equilibration reactions between magnetite and ilmenite involve the rearrangement of cations and a transformation of the oxygen sublattice from a face-centered cubic to a hexagonal close-packed framework (Gruenewaldt et al., 1995; Arguin et al., 2018). Previous solution-precipitation experiments investigating heterogeneous nucleation and crystal growth processes have found that during transformations between different crystal configurations, the crystallographic orientation of newly formed crystals is nearly parallel or slightly inclined to that of the substrate crystals (Watanabe and Funakubo, 2006; Carter and Ward, 1993). This orientation accommodates lattice misfits or dislocations and accounts for differences in surface energy between the two minerals.

The blocky or cloth-textured ilmenite crystals exsolved in Damiao magnetite formed during different stages of solid-solution evolution, yet they all crystallized along the <110> crystallographic axes (i.e., [110], [101], [011], Fig. 4). Remarkably, the blocky ilmenite exhibits both hexagonal and pyramidal shapes with threefold rotational symmetry, consistent with the c-axis orientation of magnetite crystals. This observation indicates that the (0001) basal plane of ilmenite remains parallel to the (111) plane of magnetite (Fig. 4). Tan et al. (2021) also observed consistent crystallographic orientations in magnetite-ilmenite-rutile symplectites within the Panzhihua intrusion. Therefore, the crystallographic orientation and morphological characteristics of exsolved ilmenite crystals are largely controlled by the crystalline substrate of titanomagnetite.

5.2. Subsolidus Re-equilibrium Mechanisms of Iron-Titanium Oxides

Under subsolidus temperature conditions, elemental re-equilibration reactions within iron-titanium oxides can alter the chemical compositions of magnetite and ilmenite and may lead to the exsolution of ilmenite within magnetite (Adak et al., 2021; Wei et al., 2020). In the Damiao deposit, the Fe^{3+} proportions, V/Sc and Cr/Fe ratios in magnetite-ulvöspinel and ilmenite-hematite solid solutions evolve almost synchronously (Fig. 6). This synchronicity suggests that these solid solutions share similar crystallization and compositional evolution histories in the Fe-Ti-P magma, in which fluctuations of V/Sc ratio indicate changes in oxygen fugacity during magma evolution. The Ni/Cr ratios in iron oxides decrease uniformly and gradually with magma evolution, indicating minimal influence of sulfides on the chemical

compositions of iron oxides. This observation aligns with the geological fact of low sulfide content in the Damiao deposit. Collectively, these facts suggest a high likelihood of subsolidus elemental diffusion reactions among iron oxides in the Damiao deposit.

Elemental diffusion, particularly that which conforms to valence and stoichiometric balance, provides a plausible explanation for the exsolution of ilmenite within magnetite (Tan et al., 2016, 2019; Arguin et al., 2018). Under subsolidus conditions, magnetite-ulvöspinel and ilmenite-hematite solid solutions can undergo Fe and Ti ionic re-equilibration reactions, specifically:

$$Fe^{2+} + Ti^{4+} = 2\,Fe^{3+} \quad (2)$$

The specific chemical equation is as follows:

$$Fe_2TiO_4\ (\text{in Usp-Mt}_{ss}) + Fe_2O_3\ (\text{in Hem-Ilm}_{ss}) = FeTiO_3\ (\text{in Hem-Ilm}_{ss}) + Fe_3O_4\ (\text{in Usp-Mt}_{ss}) \quad (3)$$

As temperature decreases, this reaction progressively advances toward the right, favoring the formation of solid solution end-members enriched in magnetite or ilmenite (Lindsley, 2018). The subsolidus diffusion reactions cease at approximately 500–650 °C. Low-valence, small-radius ions like Fe^{2+} and Mn^{2+} diffuse in magnetite at rates significantly higher than in ilmenite. When Fe^{2+} diffuses into ilmenite via interstitialcy diffusion and co-precipitates with Fe^{3+}, it forms magnetite exsolution; conversely, the magnetite-ulvöspinel solid solution forms ilmenite exsolution due to the loss of Fe^{2+} (Tan et al., 2016, 2019; Arguin et al., 2018).

This process indicates that the diffusion coefficients of Fe^{2+}, Fe^{3+}, and Ti^{4+} in

iron-titanium oxides under varying temperatures and oxygen fugacities are critical factors limiting the extent of reactions and the exsolution of iron-titanium oxides (Sievwright et al., 2020). Element diffusion in these oxides is influenced not only by ionic radius, valence, and ionization energy but also by factors such as rock temperature, oxygen fugacity, cooling history, mineral chemistry, and compositional gradients (Orman and Crispin, 2010; Dohmen et al., 2019). The primary diffusion mechanisms of elements in iron-titanium oxide solid solutions are interstitialcy diffusion and vacancy diffusion, with the latter being more constrained by temperature and oxygen fugacity (Aragon, 1979). In the Damiao deposit, ilmenite exhibits Fe-Mn striping, and the geochemical composition of magnetite is more uniform than that of ilmenite, indicating that the diffusion rate of elements in ilmenite is significantly lower than in magnetite (Fig. 5). Diffusion rates of different elements in magnetite-ulvöspinel can differ by up to four orders of magnitude. The approximate order is:

$$Cr < V < Ti < Al < Sc \approx Ga \approx Zr < Ni < Zn < Mn < Mg < Co < Li < Cu$$

Thus, the elemental contents of Cu, Co, Mg, Mn, and Zn are highly susceptible to the effects of diffusion re-equilibration reactions, while elements such as Cr, Ti, Sc, and Ga have slower diffusion rates, largely preserving the original characteristics of magmatic crystallization evolution (Tanner et al., 2014).

In the magnetite-ulvöspinel and ilmenite-hematite solid solutions of the Damiao deposit, the correlations of divalent ion ratios (Mg + Mn + Zn)/Fe are poor, approximately presenting as straight lines with negative slopes (Fig. 6). This pattern

confirms that elemental diffusion alters solid solution compositions due to competition among solid solution minerals for highly compatible elements. In contrast, the ratios of high-valence ions (Cr + Sc + Ga)/Fe^{3+} exhibit synchronous linear growth, reflecting the normal incorporation of compatible elements into minerals from Fe-Ti-P magma and the compositional evolution of the minerals (Fig. 6). Therefore, low-valence ions may primarily utilize the more efficient interstitialcy diffusion, while ions with higher valence and lower octahedral site preference energies are more likely to adopt the less efficient vacancy diffusion mechanism.

The diffusion re-equilibration of transition elements between iron-titanium oxides is affected not only by relative partition coefficients, but also by the relative abundances of magnetite and ilmenite (Buddington and lindsley, 1964; Charlier et al., 2015). The decoupling of geochemical characteristics of divalent ions in the two types of iron-titanium oxide solid solutions in the Damiao deposit confirms that elemental diffusion altering solid solution compositions is widespread (Fig. 6). However, magnetite dominates the iron-titanium oxides in the Damiao deposit. When unit masses of Fe^{2+} and Ti^{4+} diffuse from magnetite into ilmenite, the change in ilmenite composition is significant, whereas the change in magnetite composition is almost negligible. From the perspective of chemical reaction mass balance, even if all Fe^{3+} in the small amount of magmatically crystallized ilmenite-hematite solid solution in the Damiao deposit participates in the re-equilibration reaction, it can only account for minor proportion of the ilmenite exsolution in magnetite-ulvöspinel. Consequently, in the Damiao deposit, subsolidus re-equilibration reactions between magnetite and

ilmenite solid solutions can at most be considered a supplementary mechanism for the oxidative exsolution of magnetite.

5.3. Solubility and Diffusivity of Lithophile Elements in Fe-Ti-P Magma

In the Damiao deposit, exsolved zircon is observed at the edges of ilmenite, adjacent to altered clinopyroxene (Fig. 4). This suggests that the exsolution of zircon is likely the result of $Fe^{2+} \leftrightarrow Zr^{4+}$ exchange via diffusion between ilmenite and clinopyroxene. However, due to their valence states and ionic radii, Zr^{4+} and Si^{4+} have very slow diffusion rates in iron-titanium oxide solid solutions (Tanner et al., 2014; Tan et al., 2016). As a result, this reaction ultimately leads to the crystallization of zircon near the clinopyroxene end-member rather than within ilmenite.

An alternative explanation for the presence of zircon exsolution in ilmenite is the dissolution-saturation process within the magma (Charlier et al., 2017; Bingen et al., 2001). The solubility of elements in Fe-Ti-P magma is governed not only by temperature, pressure, and oxygen fugacity but also by the content and forms of iron-titanium oxides present. This effect is particularly pronounced for siderophile elements such as Cr, Co, Ti, Mn, and Al. Zr^{4+} and Si^{4+} in magma do not display siderophile behavior, so they are not incorporated into the composition of iron-titanium oxide solid solutions (Tanner et al., 2014; Morisset and Scoates, 2008). Therefore, the exsolution of zircon in the Damiao deposit may result from increased concentrations of Zr^{4+} and Si^{4+} in the residual melt due to the crystallization of ilmenite-hematite solid solutions, leading to their saturation and subsequent precipitation. This also explains why zircon precipitates at the edges of ilmenite rather

than at the center.

Although Al in Fe-Ti-P magma, like Zr, is not a siderophile element, it can occupy tetrahedral coordination sites in iron-titanium oxides, forming magnetite (Fe_3O_4)-hercynite ($FeAl_2O_4$) solid solutions, or it can form corundum (Al_2O_3). Exsolved corundum within magnetite has been found in the Lac Doré deposit in Canada and the Panzhihua deposit in China (Arguin et al., 2018; Tan et al., 2016). However, constrained by the pressure and oxygen fugacity conditions within the magma chamber, corundum is more likely a product of oxidized hercynite rather than directly exsolved from magma saturation. In the Damiao Fe-Ti-P magma, Al primarily exists in the form of hercynite, which can be categorized into blocky and lamellar types based on their structures and morphologies (Fig. 3). The blocky hercynite is located at the edges of ilmenite, adjacent to magnetite and titanomagnetite, indicating that the crystallization of hercynite is influenced by both ilmenite and magnetite. The eutectic temperature of magnetite-hercynite solid solutions varies between 550–860 °C depending on composition, which is significantly higher than the crystallization temperature of titanomagnetite but close to the oxidation exsolution temperature of ilmenite (Benavent et al., 2017). Therefore, the crystallization of hercynite is likely a result of increased Al content in the solid solution due to the oxidation exsolution of ilmenite. Due to its ionic radius and valence, Al has a very low diffusion rate in magnetite-titanomagnetite solid solutions. As ilmenite extends outward along the <110> crystallographic direction through oxidation exsolution, the hercynite that originally crystallized outside the ilmenite becomes enveloped by

ilmenite. In some ilmenite edges in the Damiao deposit, multiple hercynite rings are observed, indicating that continuous oxidation exsolution of ilmenite led to multiple episodes of saturation and precipitation of hercynite (Fig. 3, 5). Lamellar hercynite growing along the <010> and <001> directions in magnetite cuts across lamellar ilmenite growing along the <110> direction, suggesting that the exsolution of lamellar hercynite occurred later than that of lamellar ilmenite (Fig. 3, 5). This indicates that hercynite exsolution in the Damiao deposit persisted from approximately 850 °C down to around 500 °C, traversing the eutectic line of magnetite-hercynite. This finding provides new evidence for studying the cooling history of the Damiao intrusion.

5.4. Cooling History of the Damiao Fe-Ti-P Oxide Rocks and Implications for the Immiscible Origin of Nelsonitic Melts

The cooling history of the Damiao complex can be constrained by the geological processes discussed in previous sections, namely, the redox reactions and subsolidus equilibrium reactions among iron-titanium oxides or between these oxides and silicate minerals. The direction of each process, along with the temperature, pressure, and oxygen fugacity ranges within which the substances remain stable, can be determined by the Gibbs free energy of the corresponding chemical reactions.

$$\Delta G = \sum_1^n v_i^j \cdot \mu_i^j \leq 0 \quad (4)$$

Here, ν and μ represent the stoichiometric coefficients and chemical potentials, respectively. The chemical potential is calculated using the following equation:

$$\mu_i^j = \Delta H_{i,T_r,P_r}^{o,j} - T \cdot S_{i,T_r,P_r}^{o,j} + \int_{T_r}^{T} C_P \cdot dT - T \cdot \int_{T_r}^{T} \frac{C_P}{T} \cdot dT + \int_{P_r}^{P} V_{i,T,P}^{o,j} \cdot dP + R \cdot$$

$T \cdot lna_i^j$ (5)

In this equation, ΔH^0 and S^0 are the standard molar enthalpy and entropy of substance i under standard conditions (T_r, P_r). C_P and $V_{i,T,P}$ represent the heat capacity and molar volume of substance i at specific temperatures and pressures, respectively, and α denotes the activity of substance i. The standard-state thermodynamic parameters and activity data of iron-titanium oxides involved in these reactions are primarily referenced from the standards published by the U.S. Geological Survey in 1995, as well as the QUILF and WinMLgob databases and programs (Andersen et al., 1993; Yavuz, 2021). Experimental methods mainly involve phase equilibrium and calorimetry to measure entropy, enthalpy, and heat capacity. The databases and computational programs encompass numerous thermodynamic models of iron-titanium oxide solid solutions accumulated over the years (Lindsley and Frost 1992; Andersen et al. 1993; Sauerzapf et al., 2008; Ghiorso and Evans, 2008). Additionally, the entropy and enthalpy changes resulting from the structural transition of ilmenite-hematite solid solutions from $R\bar{3}C$ to $R\bar{3}$ with temperature are primarily referenced from Richardson et al. (2000). The thermal expansion and compression coefficients of iron-titanium oxides are based on the least-squares fitting results by Wechsler and Prewitt (1984). Errors in temperature, pressure, oxygen fugacity, and chemical composition are incorporated into the Gibbs free energy calculations throughout the computational process.

This study primarily infers the cooling history of the intrusion using mineral compositions from Damiao Fe-Ti-P ores, nelsonites, and gabbronorites. The main

evidence includes: 1. The iron-titanium oxides in the Damiao deposit are predominantly magnetite, with exsolved blocky, lamellar, and cloth-textured ilmenite exhibiting relatively uniform compositions (Fig. 7); 2. The geochemical characteristics of magnetite, ilmenite, and clinopyroxene in the Damiao intrusion indicate elemental diffusion and compositional equilibration processes among iron-titanium oxides and between these oxides and silicate minerals (Fig. 7); 3. The oxygen fugacity–temperature evolution curve calculated using magnetite and ilmenite compositions from Damiao via the QUILF program approximately coincides with the Usp=30% isopleth (Fig. 7). Therefore, the intersection points of the oxygen fugacity–temperature evolution curve of the Damiao deposit with the thermodynamic equation curves in the Fe-Ti-Si system approximately reflect the temperature and oxygen fugacity ranges of the corresponding processes occurring in the magma chamber. Meanwhile, the exsolution temperatures of Al hercynite can also be determined based on the solvus lines of the Fe_2TiO_4–Fe_3O_4, $FeTiO_3$–Fe_2O_3, and Fe_3O_4–$FeAl_2O_4$ solid solutions.

The geochemical characteristics of iron-titanium oxides in the Damiao deposit confirm that the initial conditions of the Fe-Ti-P magma were relatively reducing. The evolution curve of these oxides lies below the magnetite–hematite (MH) buffer curve, indicating the cooling history was dominated by magnetite (Fig. 7). Subsolidus elemental equilibrium between magnetite and ilmenite is primarily achieved through the diffusion of Fe and Ti. Although thermodynamic equations suggest this reaction is independent of oxygen fugacity, the chemical compositions of oxide mineral

assemblages (e.g., magnetite–hematite and ulvöspinel–ilmenite buffers) are constrained by oxygen fugacity. At low temperatures, the solubility of Ti in magnetite decreases, and the elemental equilibrium between iron-titanium oxides tends to form relatively pure magnetite and ilmenite end-members (Evans et al., 2006; Tan et al., 2016). The thermodynamic curve of this reaction approximates the MH buffer curve. At high temperatures, the solubility of Ti in magnetite-ulvöspinel solid solutions increases, and the influence of oxygen fugacity on this reaction gradually diminishes, eventually becoming negligible above 1000 °C (Frost, 1991).

Calculations of Damiao oxide composition using the QUILF program indicate that elemental diffusion between iron-titanium oxides begins to occur at temperatures of 700-800 °C and oxygen fugacity conditions from QFM to QFM–1 (Fig. 7). These conditions are close to those of the oxidation process of ulvöspinel. Once oxidation exsolution begins, the insoluble Ti in magnetite finds suitable positions without needing to diffuse out of the magnetite solid solution. Therefore, the compositions of magnetite-ulvöspinel and exsolved ilmenite can approximately indicate the temperature and oxygen fugacity conditions where elemental diffusion processes terminate. However, due to the high valence and large ionic radius of Ti^{4+}, its diffusion effect in magnetite is minimal (Tanner et al., 2014). When the temperature drops below 600 °C, the diffusion of Ti ions nearly ceases, making it unrealistic to calculate the exact conditions for the termination of elemental diffusion based solely on oxide compositions.

In the Damiao deposit, oxidation of magnetite leads to significant differences in

the compositions and structures of ilmenite exsolutions (Fig. 7). By estimating the composition of titanomagnetite and its crystallization temperature (approximately 800–850 °C) through mass balance using the compositions of magnetite and ilmenite exsolutions, we find that continuous crystallization of iron-titanium oxides causes the magma's temperature to gradually decrease. Elemental equilibrium processes occur between magnetite and ilmenite, followed by oxidation exsolution of ulvöspinel to form ilmenite due to increased oxygen fugacity. Blocky and lamellar ilmenite form above the solid solution solvus at temperatures around 700 °C, while cloth-textured ilmenite forms below the solvus at temperatures around 530 °C (Fig. 7). Various factors might account for the changes in oxygen fugacity of the Fe-Ti-P magma in Damiao. One possibility is the assimilation and contamination of wall rocks, enriching the magma with CO_2, H_2S, and H_2O, which could serve as oxygen sources. Recent studies on magmatic melt inclusions have supported this hypothesis (Iacono-Marziano, 2020). Another possibility is the mixing of magmas with different degrees of evolution or varying oxygen fugacities (Cottrell et al., 2021).

The main mineral assemblage of the Damiao deposit consists of iron-titanium oxides, olivine, and clinopyroxene. Therefore, the elemental equilibrium (QUILF) and redox reactions (QFM) between iron-titanium oxides and silicate minerals need to be incorporated into the evolution history calculations. The elemental equilibrium reaction in the QUILF thermodynamic equations does not involve oxygen, but the compositions of the iron-titanium oxide and olivine solid solutions are influenced by changes in the magma's oxygen fugacity. Under high oxygen fugacity, the magma

tends to form magnetite, hematite, and forsterite end-members; under low oxygen fugacity, the opposite occurs. At high temperatures, the influence of oxygen fugacity on the elemental equilibrium reaction is minimal, and the reaction terminates when temperatures exceed olivine's crystallization temperature (Pang et al., 2008; Arguin et al., 2018). At low temperatures, the solubility of Ti in titanomagnetite decreases, leading to reduced ulvöspinel activity and increased magnetite activity. The reaction between iron-titanium oxides and SiO_2 in the magma gradually shifts from an elemental equilibrium reaction to a redox reaction (QFM). Calculations indicate that iron-titanium oxides react with SiO_2 in the magma to form olivine at around 700-800°C (Fig. 7).

The oxide-apatite gabbronorites in the Damiao deposit mainly outcrop as veins or pseudo-layers, with iron-titanium oxides uniformly distributed among silicate interstitial phases, displaying cumulate textures (He et al., 2016, 2019). This indicates that Fe-Ti oxide crystallization was concurrent with or slightly later than that of silicate minerals. Oxygen fugacity during the crystallization of oxide-apatite gabbronorites, calculated from magnetite and ilmenite compositions, is about QFM, significantly higher than the oxygen fugacity during the crystallization of Fe-Ti-P ores, providing constraints on the genesis of the Damiao deposit. The Damiao deposit primarily formed from ferrodioritic magmas (Chen et al., 2013; He et al., 2016). The oxide-apatite gabbronorite resulted from Fe-Ti-P-rich residual melts after plagioclase and pyroxene fractional crystallization from the ferrodioritic magma. This residual melt evolved into Fe-Ti-P-rich melts through immiscibility, eventually crystallizing to

form oxide ores (Chen et al., 2013; He et al., 2016). Therefore, the oxide-apatite gabbronorite and Fe-Ti-P ores can reflect changes in the parent magma's composition and oxygen fugacity conditions before and after immiscibility. Experimental study indicates that increasing magma oxygen fugacity can expand the compositional range over which immiscibility occurs, making Fe-rich melts more likely to separate from silicic magma (Hou et al., 2018). Combined with our calculations of the ferrodioritic magma's oxygen fugacity, this suggests that oxygen fugacity played a crucial role in the immiscibility process of Fe-Ti-P melts in the Damiao deposit.

6. Conclusion:

The Damiao Fe-Ti-P deposit within the Damiao anorthosite complex in northeastern China offers important insights into the formation processes of Fe-Ti oxide ores in mafic intrusions. Through detailed petrographic observations and geochemical analyses, this study reveals that the diverse ilmenite exsolution textures present in titanomagnetite result from a complex interplay of magmatic events and subsolidus transformations. The variety of ilmenite exsolution textures, including blocky, lamellar, and cloth-like forms, originated from multiple mechanisms operating under different temperature regimes and oxygen fugacity conditions. The primary mechanisms identified are magmatic oxidation events (oxy-exsolution) due to the oxidation of titanomagnetite, subsolidus re-equilibration between magnetite and ilmenite facilitated by elemental diffusion (notably of Fe, Ti, Cr, Co, and Ni), and exsolution induced by rapid cooling leading to lattice defects. Thermodynamic modeling supports these findings, indicating that these exsolution textures formed

both above and below the solid solution solvus at varying oxygen fugacities. The influence of variable oxygen fugacity, coupled with the cooling trajectory of the ferrodioritic magma, played a pivotal role in controlling the mineralogical and textural evolution of the deposit. This underscores the significance of fluctuating redox conditions during the cooling and crystallization of the magma. Additional mineralogical transformations were observed, such as the exsolution of zircon at ilmenite grain boundaries, attributed to interactions between ilmenite and adjacent clinopyroxene. The formation of hercynite is associated with increased aluminum content in the solid solution resulting from the oxidation of ilmenite. These processes highlight the role of elemental exchanges and subsolidus reactions in the evolution of the deposit's mineralogy. The reconstructed cooling history suggests that the Fe-Ti oxide ores crystallized from a ferrodioritic magma. An increase in oxygen fugacity during magma evolution appears to have been a crucial factor, possibly promoting immiscibility and leading to the segregation of Fe-Ti-P-rich melts. This process ultimately resulted in the formation of nelsonitic ores, which manifest as stratiform-like bodies, lenses, or veins sharply contrasting with the surrounding anorthosite and gabbronorite.

References

Adak, S., et al. (2021). "Textural re-equilibration, hydrothermal alteration and element redistribution in Fe-Ti oxide pods, Singhbhum Shear Zone, eastern India." Geochemistry 81(1): 125679.

Andersen, D. J., et al. (1993). "QUILF: A pascal program to assess equilibria among Fe Mg Mn Ti oxides, pyroxenes, olivine, and quartz." Computers & Geosciences 19(9): 1333-1350.

ARAGON, R. (1979). Chemical equilibria and kinetics associated with reactions in the magnetite-

ulvospinel system, Purdue University.

Arguin, J.-P., et al. (2018). "An integrated model for ilmenite, Al-spinel, and corundum exsolutions in titanomagnetite from oxide-rich layers of the Lac Doré Complex (Québec, Canada)." Minerals 8(11): 476.

Bhattacharjee, C. and S. K. Mondal (2021). "Geochemistry of Fe-Ti oxide and sulfide minerals in gabbroic rocks and magnetitite of the Archean Mayurbhanj mafic complex (eastern India): Magma fractionation, thermometry and oxygen fugacity of re-equilibration, and implications for Ni-Cu mineralization." Ore Geology Reviews 131: 104005.

Bingen, B., et al. (2001). "Ilmenite as a source for zirconium during high-grade metamorphism? Textural evidence from the Caledonides of Western Norway and implications for zircon geochronology." Journal of Petrology 42(2): 355-375.

Buddington, A. F. and D. Lindsley (1964). "Iron-titanium oxide minerals and synthetic equivalents." Journal of Petrology 5(2): 310-357.

Carter, P. W. and M. D. Ward (1993). "Topographically directed nucleation of organic crystals on molecular single-crystal substrates." Journal of the American Chemical Society 115(24): 11521-11535.

Charlier, B., et al. (2015). "Fe – Ti – V – P ore deposits associated with Proterozoic massif-type anorthosites and related rocks." Earth-Science Reviews 141: 56-81.

Charlier, B., et al. (2007). "Ilmenite composition in the Tellnes Fe – Ti deposit, SW Norway: fractional crystallization, postcumulus evolution and ilmenite – zircon relation." Contributions to Mineralogy and Petrology 154: 119-134.

Chen, W. T., et al. (2013). "Differentiation of nelsonitic magmas in the formation of the~ 1.74 Ga Damiao Fe – Ti – P ore deposit, North China." Contributions to Mineralogy and Petrology 165: 1341-1362.

Cottrell, E., et al. (2021). "Oxygen fugacity across tectonic settings." Magma redox geochemistry: 33-61.

Dohmen, R., et al. (2019). "Diffusion of Zr, Hf, Nb and Ta in rutile: effects of temperature, oxygen fugacity, and doping level, and relation to rutile point defect chemistry." Physics and Chemistry of Minerals 46: 311-332.

Evans, B. W., et al. (2006). "Experimental determination of coexisting iron – titanium oxides in the systems FeTiAlO, FeTiAlMgO, FeTiAlMnO, and FeTiAlMgMnO at 800 and 900 C, 1 – 4 kbar, and relatively high oxygen fugacity." Contributions to Mineralogy and Petrology 152(2): 149-167.

Frost, B. R. (1991). "Magnetic petrology; factors that control the occurrence of magnetite in crustal rocks." Reviews in Mineralogy and Geochemistry 25(1): 489-509.

Gao, W., et al. (2019). "Nanoscale study of titanomagnetite from the Panzhihua Layered Intrusion, Southwest China: Multistage exsolutions record ore formation." Minerals 9(9): 513.

Ghiorso, M. S. and B. W. Evans (2008). "Thermodynamics of rhombohedral oxide solid solutions and a revision of the Fe-Ti two-oxide geothermometer and oxygen-barometer." American Journal of science 308(9): 957-1039.

Gorbatova, E., et al. (2021). "Solid-Phase Transformations of Titanomagnetite and Ilmenite during Oxidizing Roasting of Disseminated Titanomagnetite – Ilmenite Ore at the Medvedevskoe Deposit and Certain Geological Events (Southern Urals)." Geology of Ore Deposits 63(5): 431-453.

Harrison, R. J. and A. Putnis (1997). "Interaction between exsolution microstructures and magnetic properties of the magnetite-spinel solid solution." American Mineralogist 82(1-2): 131-142.

He, H.-L., et al. (2019). "Lower crustal contribution to the magma formation of the Damiao massif-type anorthosite, North China Craton: Evidence from zircon Hf-O isotopes." Precambrian Research 332: 105396.

He, H.-L., et al. (2016). "Origin of nelsonite and Fe − Ti oxides ore of the Damiao anorthosite complex, NE China: Evidence from trace element geochemistry of apatite, plagioclase, magnetite and ilmenite." Ore Geology Reviews 79: 367-381.

Hou, T., et al. (2018). Immiscible hydrous Fe − Ca − P melt and the origin of iron oxide-apatite ore deposits. Nat Commun 9: 1415.

Iacono-Marziano, G. (2020). "Interactions between magmas and host sedimentary rocks: a review of their implications in magmatic processes (magma evolution, gas emissions and ore processes)."

Khedr, M. Z., et al. (2024). "Mineralogy and Geochemistry of Titaniferous Iron Ores in El-Baroud Layered Gabbros: Fe-Ti Ore Genesis and Tectono-Metallogenetic Setting." Minerals 14(7): 679.

Lattard, D. (1995). "Experimental evidence for the exsolution of ilmenite from titaniferous spinel." American Mineralogist 80(9-10): 968-981.

Lee, J. H., et al. (2022). "Whole-rock geochemistry and mineral compositions of gabbroic rocks and the associated Fe − Ti (− V) oxide deposit in the Gonamsan intrusion, South Korea." Ore Geology Reviews 148: 105054.

Li, H., et al. (2014). "Alteration of the Damiao anorthosite complex in the northern North China Craton: Implications for high-grade iron mineralization." Ore Geology Reviews 57: 574-588.

Li, L. X., et al. (2019). "The link between an anorthosite complex and underlying olivine − Ti-magnetite-rich layered intrusion in Damiao, China: insights into magma chamber processes in the formation of Proterozoic massif-type anorthosites." Contributions to Mineralogy and Petrology 174: 1-21.

Li, L.-X., et al. (2019). "Role of fluids in Fe − Ti − P mineralization of the Proterozoic Damiao anorthosite complex, China: Insights from baddeleyite − zircon relationships in ore and altered anorthosite." Ore Geology Reviews 115: 103186.

Li, Y., et al. (2024). "Prolonged evolution of syn-collisional progressive deformation of the Trans-North China Orogen: Structural and geochronological evidence from the Xiaoqinling region, central China." Gondwana Research 129: 332-354.

Lilova, K. I., et al. (2012). "Thermodynamics of the magnetite-ulvöspinel (Fe3O4-Fe2TiO4) solid solution." American Mineralogist 97(8-9): 1330-1338.

Lindsley, D. H. (2018). Oxide minerals: petrologic and magnetic significance, Walter de Gruyter GmbH & Co KG.

Lindsley, D. H. and B. R. Frost (1992). "Equilibria among Fe-Ti oxides, pyroxenes, olivine, and quartz: Part I. Theory." American Mineralogist 77(9-10): 987-1003.

Liu, J.-f., et al. (2016). "Late Paleoproterozoic tectonic setting of the northern margin of the North China Craton: Constraints from the geochronology and geochemistry of the mangerites in the Longhua and Jianping areas." Precambrian Research 272: 57-77.

Lusted, K. (2019). Textures of Titaniferous Magnetite within the Bushveld Igneous Complex

South Africa, University of Pretoria (South Africa).
Morisset, C.-E. and J. S. Scoates (2008). "Origin of zircon rims around ilmenite in mafic plutonic rocks of Proterozoic anorthosite suites." The Canadian Mineralogist 46(2): 289-304.
Noh, J., et al. (2015). "Magnetite Fe3O4 (111) surfaces: impact of defects on structure, stability, and electronic properties." Chemistry of Materials 27(17): 5856-5867.
Otto, T. (2017). Texture development in titaniferous magnetites found in Layer 21 in the Bushveld Igneous Complex, South Africa, University of Pretoria (South Africa).
Özdemir, Ö. and D. J. Dunlop (1997). "Effect of crystal defects and internal stress on the domain structure and magnetic properties of magnetite." Journal of Geophysical Research: Solid Earth 102(B9): 20211-20224.
Pang, K.-N., et al. (2008). "Origin of Fe − Ti oxide ores in mafic intrusions: evidence from the Panzhihua intrusion, SW China." Journal of Petrology 49(2): 295-313.
Pang, K.-N., et al. (2010). "Flood basalt-related Fe − Ti oxide deposits in the Emeishan large igneous province, SW China." Lithos 119(1-2): 123-136.
Paton, C., et al. (2011). "Iolite: Freeware for the visualisation and processing of mass spectrometric data." Journal of Analytical Atomic Spectrometry 26(12): 2508-2518.
Pearce, C. I., et al. (2010). "Fe site occupancy in magnetite-ulvospinel solid solutions: A new approach using X-ray magnetic circular dichroism." American Mineralogist 95(4): 425-439.
Price, G. D. (1981). "Subsolidus phase relations in the titanomagnetite solid solution series." American Mineralogist 66(7-8): 751-758.
Qi, L. and M.-F. Zhou (2008). "Platinum-group elemental and Sr − Nd − Os isotopic geochemistry of Permian Emeishan flood basalts in Guizhou Province, SW China." Chemical Geology 248(1-2): 83-103.
Robie, R. A., et al. (1978). Thermodynamic properties of minerals and related substances at 298.15 K and 1 bar (105 pascals) pressure and at higher temperatures, Department of the Interior, US Geological Survey.
Sauerzapf, U., et al. (2008). "The titanomagnetite − ilmenite equilibrium: new experimental data and thermo-oxybarometric application to the crystallization of basic to intermediate rocks." Journal of Petrology 49(6): 1161-1185.
She, Y.-W., et al. (2014). "The formation of P-rich Fe − Ti oxide ore layers in the Taihe layered intrusion, SW China: implications for magma-plumbing system process." Ore Geology Reviews 57: 539-559.
Sievwright, R., et al. (2020). "Diffusion and partition coefficients of minor and trace elements in magnetite as a function of oxygen fugacity at 1150 °C." Contributions to Mineralogy and Petrology 175: 1-21.
Tan, W., et al. (2022). "Magnetite-rutile symplectite in ilmenite records magma hydration in layered intrusions." American Mineralogist: Journal of Earth and Planetary Materials 107(3): 395-404.
Tanner, D., et al. (2014). "Trace element stratigraphy of the Bellevue Core, Northern Bushveld: multiple magma injections obscured by diffusive processes." Journal of Petrology 55(5): 859-882.
Teng, X., et al. (2015). "Devonian magmatism associated with arc-continent collision in the northern North China Craton: evidence from the Longwangmiao ultramafic intrusion in the Damiao area." Journal of Asian Earth Sciences 113: 626-643.

Van Orman, J. A. and K. L. Crispin (2010). "Diffusion in oxides." Reviews in Mineralogy and Geochemistry 72(1): 757-825.

Villanova-de-Benavent, C., et al. (2017). "Fe − Ti (− V) oxide deposits of the Kunene Anorthosite Complex (SW Angola): mineralogy and thermo-oxybarometry." Minerals 7(12): 246.

Von Gruenewaldt, G., et al. (1985). "Exsolution features in titanomagnetites from massive magnetite layers and their host rocks of the upper zone, eastern Bushveld Complex." Economic Geology 80(4): 1049-1061.

Wan, Y., et al. (2013). "Is the Ordos block Archean or Paleoproterozoic in age? Implications for the Precambrian evolution of the North China Craton." American Journal of science 313(7): 683-711.

Wang, M., et al. (2017). "The origin of nelsonite constrained by melting experiment and melt inclusions in apatite: The Damiao anorthosite complex, North China Craton." Gondwana Research 42: 163-176.

Watanabe, T. and H. Funakubo (2006). "Controlled crystal growth of layered-perovskite thin films as an approach to study their basic properties." Journal of applied physics 100(5).

Wechsler, B. A., et al. (1984). "Crystal structure and cation distribution in titanomagnetites (Fe3-xTixO4)." American Mineralogist 69(7-8): 754-770.

Wei, Y., et al. (2020). "Geochemistry and iron isotope systematics of coexisting Fe-bearing minerals in magmatic FeTi deposits: a case study of the Damiao titanomagnetite ore deposit, North China Craton." Gondwana Research 81: 240-251.

Yan, Y.-Q., et al. (2025). "Carboniferous, not Paleoproterozoic, eclogite-facies metamorphism in the northern North China Craton as revealed by in situ garnet Lu-Hf and U-Pb geochronology." Earth and Planetary Science Letters 653: 119207.

Yang, Q.-Y., et al. (2014). "Late Paleoproterozoic charnockite suite within post-collisional setting from the North China Craton: petrology, geochemistry, zircon U − Pb geochronology and Lu − Hf isotopes." Lithos 208: 34-52.

Yavuz, F. (2021). "WinMIgob: A Windows program for magnetite-ilmenite geothermometer and oxygen barometer." Journal of Geosciences 66(1): 51-70.

Zhai, M. and M. Santosh (2013). "Metallogeny of the North China Craton: link with secular changes in the evolving Earth." Gondwana Research 24(1): 275-297.

Zhao, T.-P., et al. (2009). "Geochemical and Nd − Hf isotopic constraints on the origin of the~ 1.74-Ga Damiao anorthosite complex, North China Craton." Lithos 113(3-4): 673-690.

FIGURE CAPTIONS

Figure 1. Geologic Map of the Damiao Anorthosite Complex and Fe–Ti Oxide Orebodies

Figure 2. Photomicrographs of the Damiao Rocks and Ores. a. Massive Fe − Ti Ore: Coarse-grained euhedral magnetite and ilmenite with sharp boundaries. b. Nelsonite: Euhedral magnetite, ilmenite, and euhedral to subhedral apatite

making up to 90% of the rock. c. Gabbronorite: Plagioclase, oxides, and euhedral to subhedral apatite. d. Gabbro-Nelsonite: Interstitial anhedral plagioclase among Fe − Ti oxides and euhedral to subhedral apatite.

Figure 3. EPMA Element Map of the exsolved Ilmenite and Titanomagnetite in Fe-Ti Ore from the Damiao Deposit, which illustrates the distribution of various major elements between the mineral phases. The relative concentrations of the elements are semiquantitative. hercynite is distributed around the edges of ilmenite. Granule and thick ilmenite lamellae and pleonaste particles in the host magnetite

Figure 4. EPMA Element Map of the exsolved zircon and ilmenite in Fe-Ti Ore from the Damiao Deposit. Zircon is distributed around the edges of ilmenite.

Figure 5. EPMA Element Map of the exsolved Ilmenite and Titanomagnetite in Fe-Ti Ore from the Damiao Deposit, Trellis-type lamellae of Ilmenite-E1 parallel to three sets of {111} lattice planes of the magnetite structure;

Figure 6. Bi-elemental variation diagrams of titanomagnetite and ilmenite from various ores/rocks.

Figure 7. oxygen fugacity-temperature diagram showing inferred cooling trend for Fe^Ti oxides in the Damiao deposit.

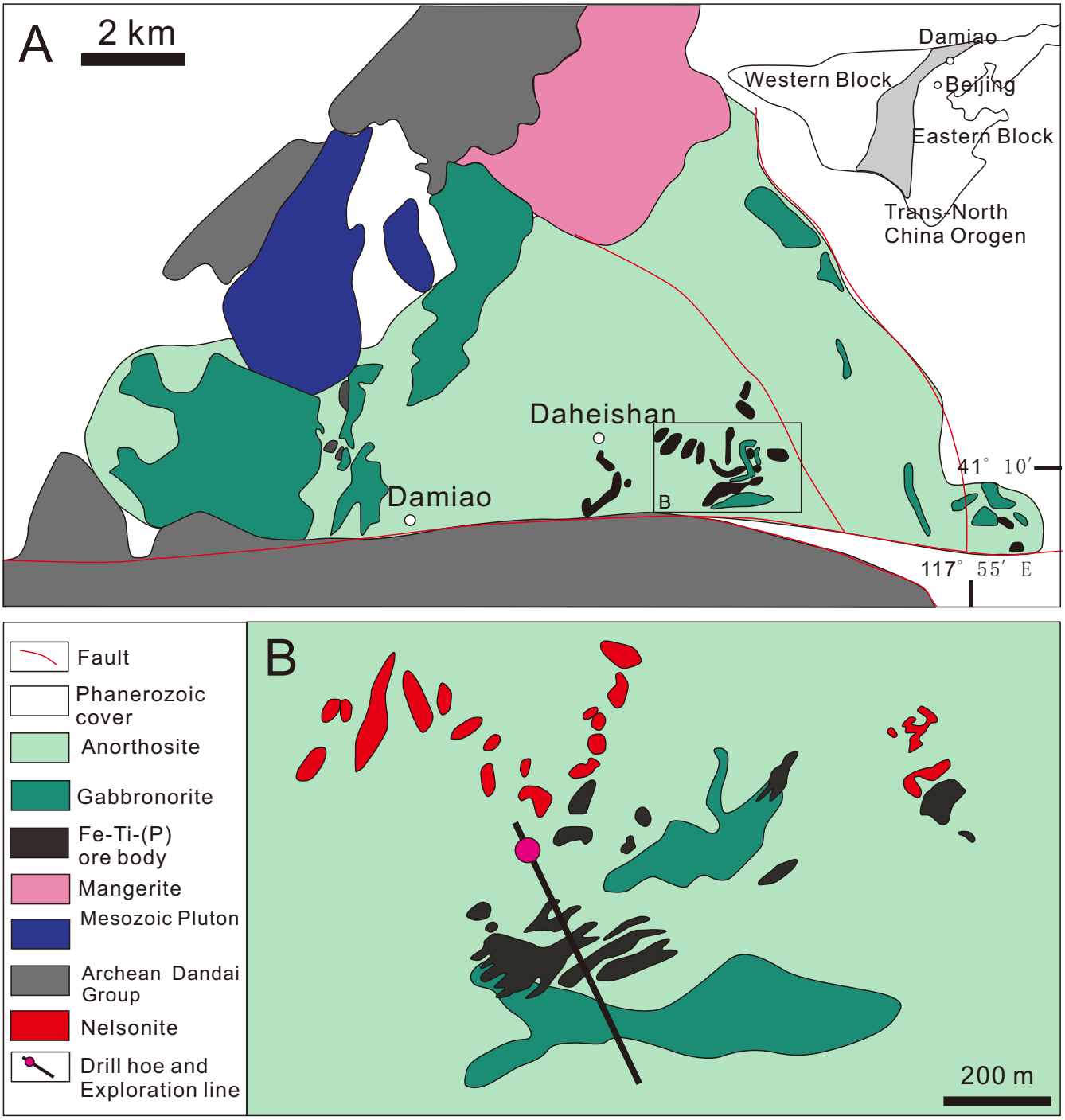
A
2 km
Damiao
Western Block
Beijing
Eastern Block
Trans-North
China Orogen
Daheishan
Damiao
B
41° 10′
117° 55′ E
Fault
Phanerozoic cover
Anorthosite
Gabbronorite
Fe-Ti-(P) ore body
Mangerite
Mesozoic Pluton
Archean Dandai Group
Nelsonite
Drill hoe and Exploration line
B
200 m

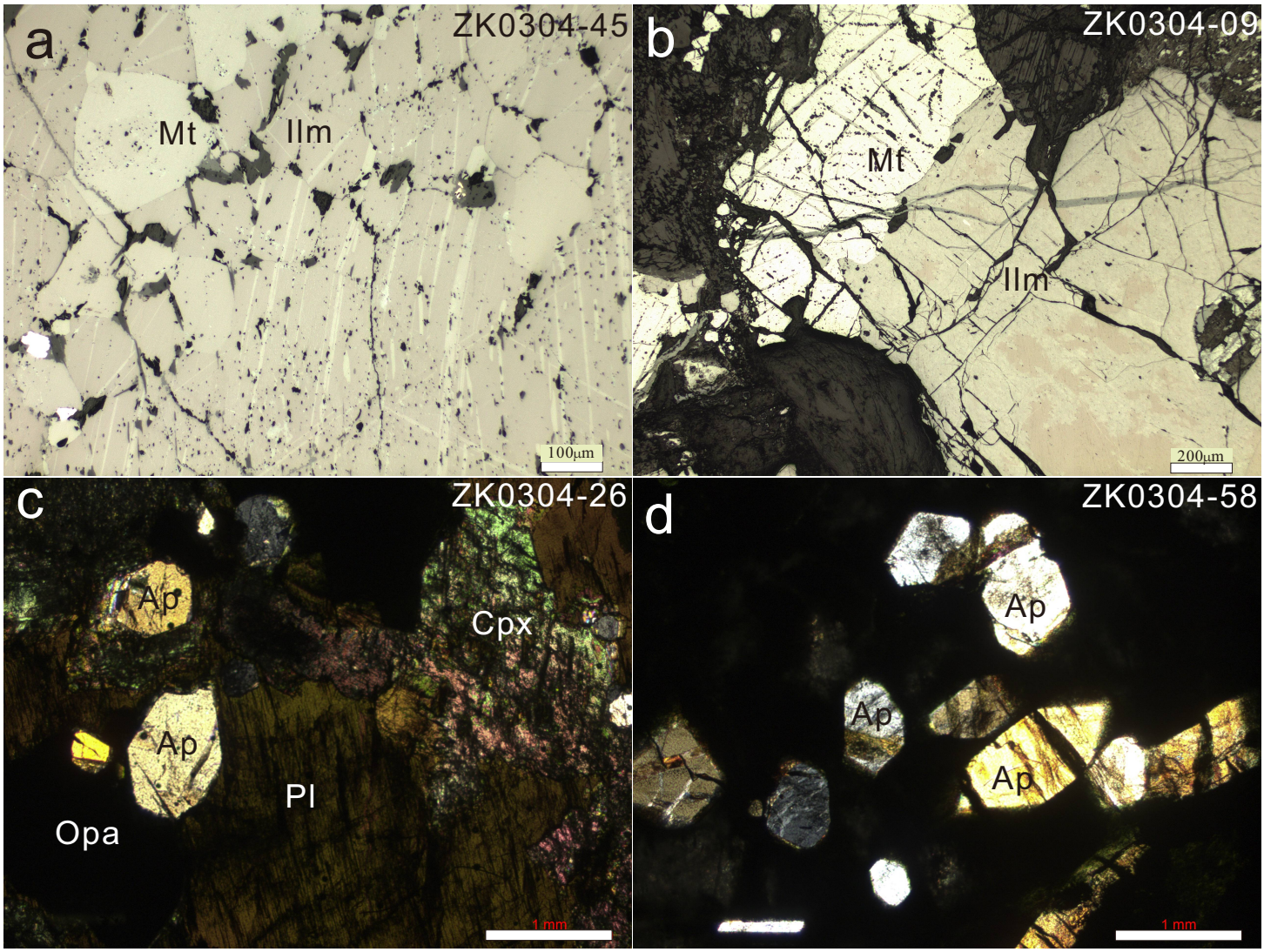
a
ZK0304-45
Mt
Ilm
100μm
b
ZK0304-09
Mt
Ilm
200μm
c
ZK0304-26
Ap
Cpx
Ap
Pl
Opa
1 mm
d
ZK0304-58
Ap
Ap
Ap
1 mm

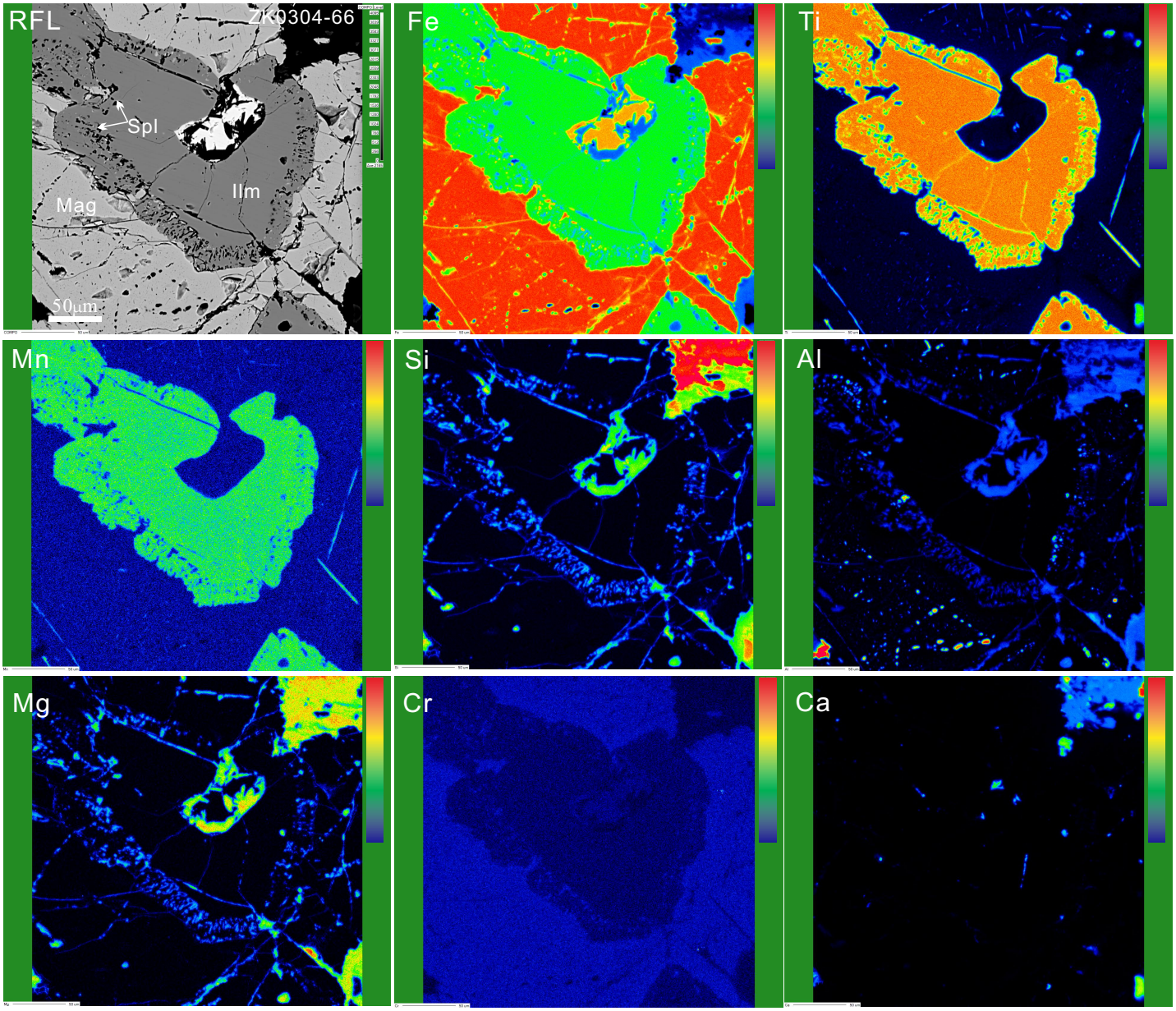
RFL
ZK0304-66
Spl
Ilm
Mag
50μm
Fe
Ti
Mn
Si
Al
Mg
Cr
Ca

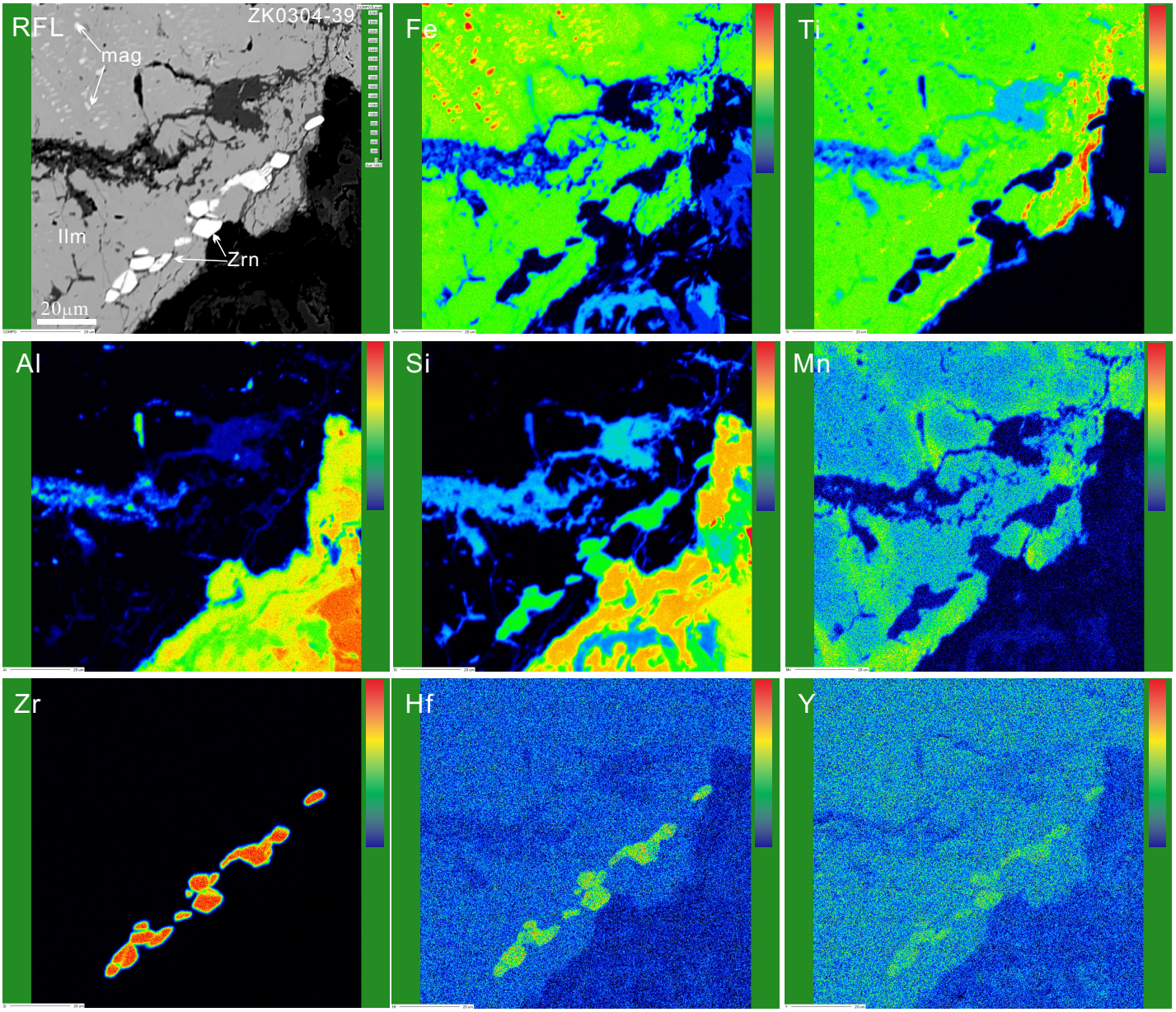
RFL
ZK0304-39
mag
Ilm
Zrn
20μm
Fe
Ti
Al
Si
Mn
Zr
Hf
Y

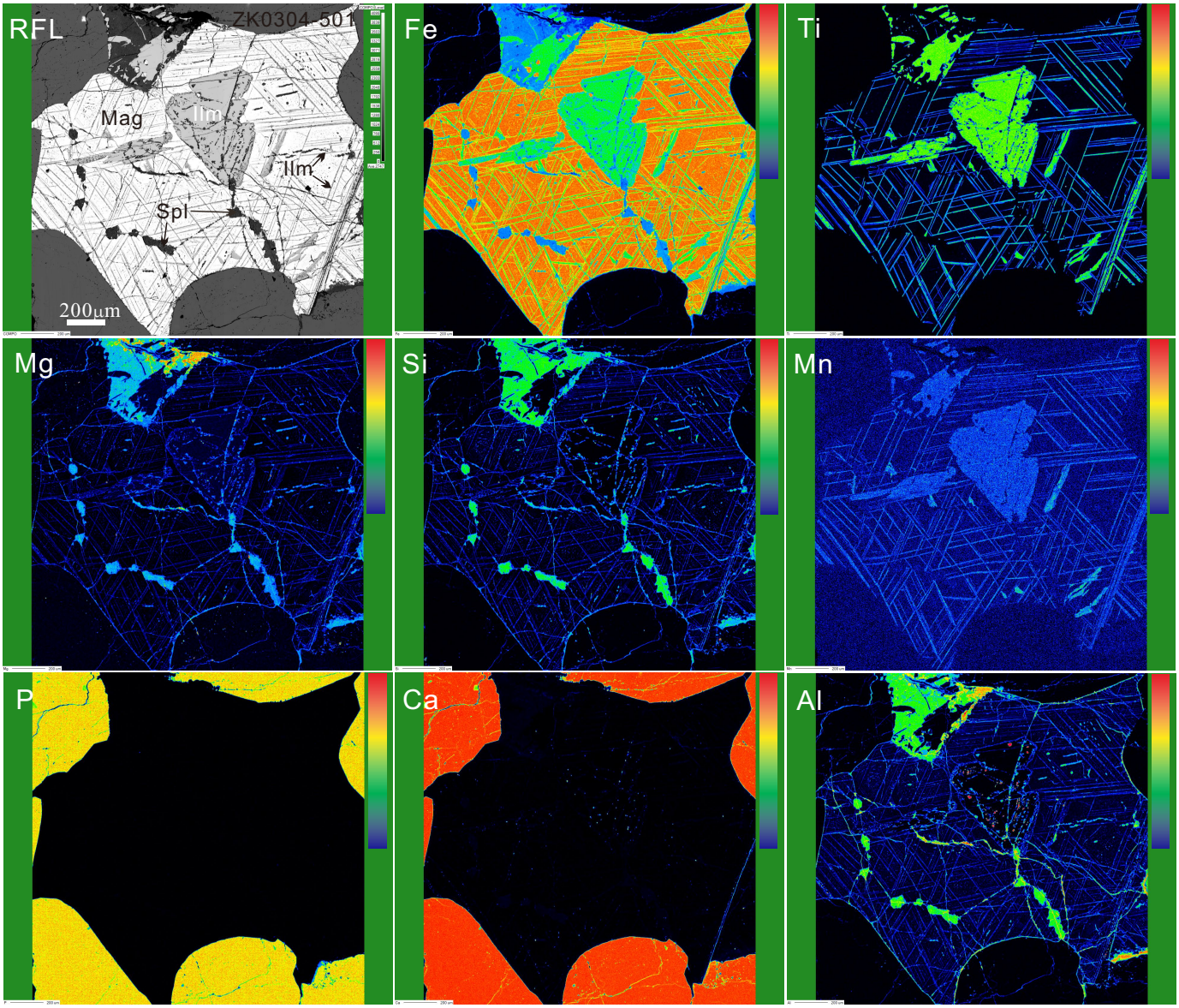
RFL
ZK0304-501
Mag
Ilm
Ilm
Spl
200μm
Fe
Ti
Mg
Si
Mn
P
Ca
Al

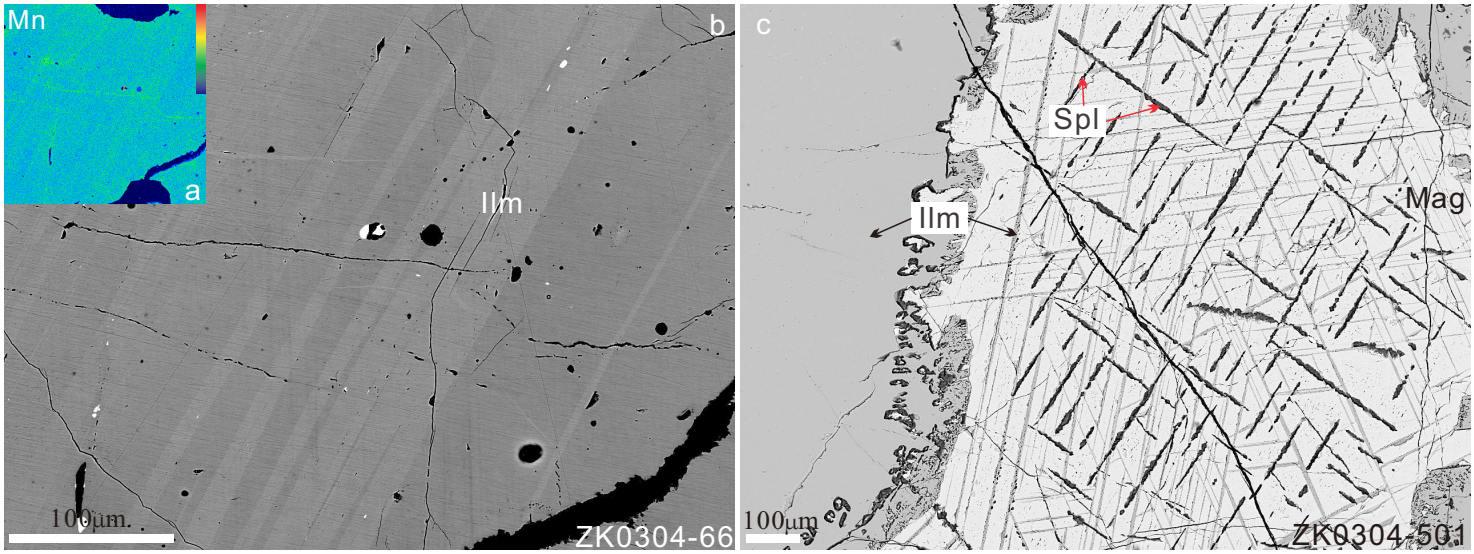
Mn
a
b
Ilm
100μm.
ZK0304-66
c
Spl
Ilm
Mag
100μm
ZK0304-501

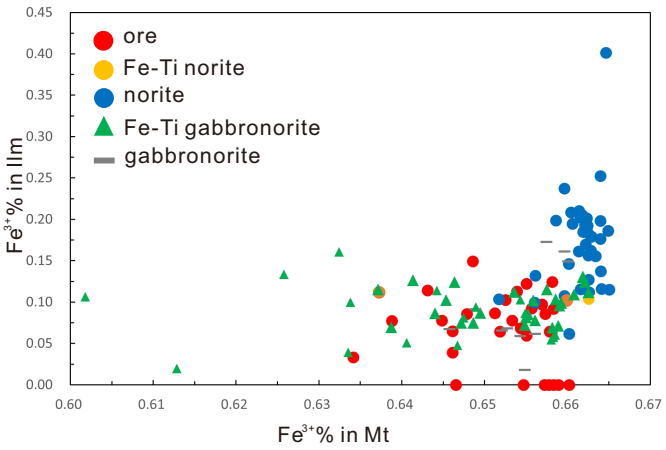
ore
Fe-Ti norite
norite
Fe-Ti gabbronorite
gabbronorite
Fe3+% in Ilm
Fe3+% in Mt

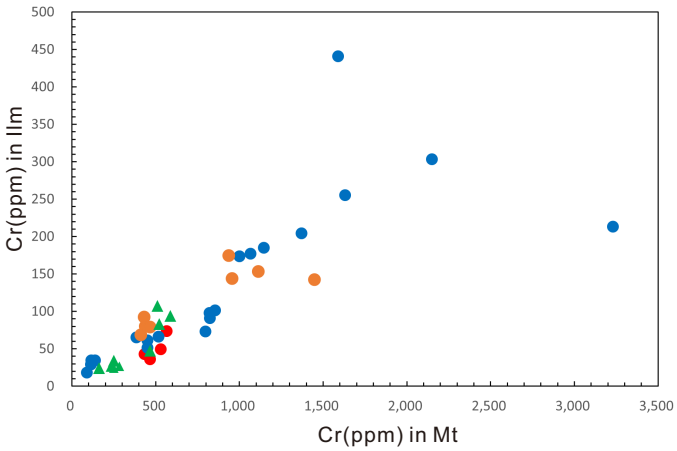
Cr(ppm) in Ilm
Cr(ppm) in Mt

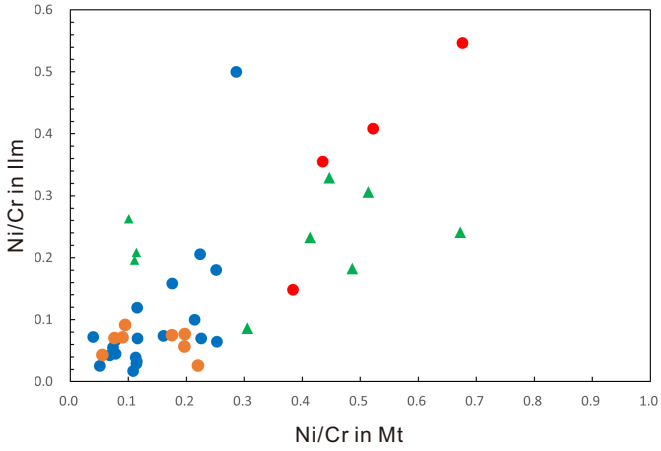
Ni/Cr in Ilm
Ni/Cr in Mt

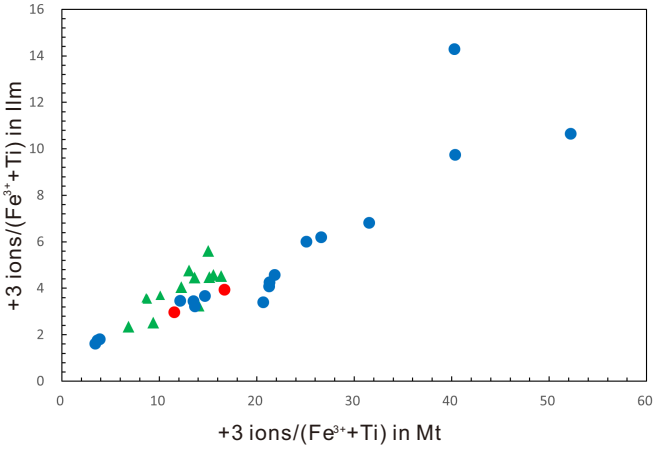
+3 ions/(Fe3++Ti) in Ilm
+3 ions/(Fe3++Ti) in Mt

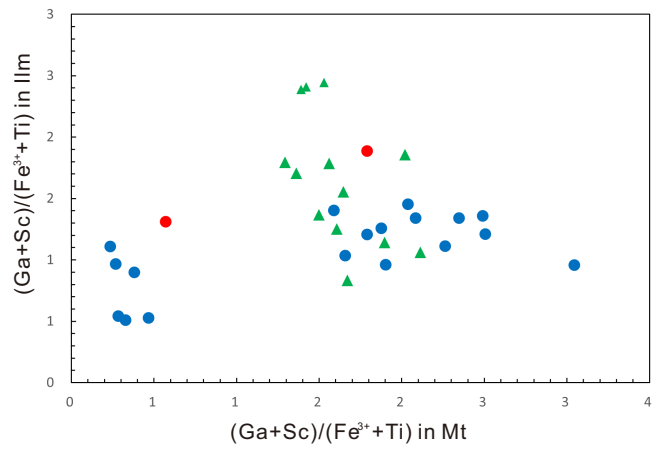
(Ga+Sc)/(Fe3++Ti) in Ilm
(Ga+Sc)/(Fe3++Ti) in Mt

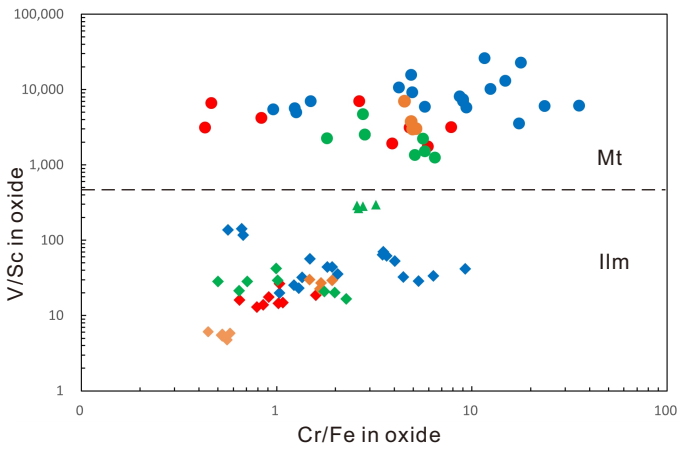
Mt
Ilm
V/Sc in oxide
Cr/Fe in oxide

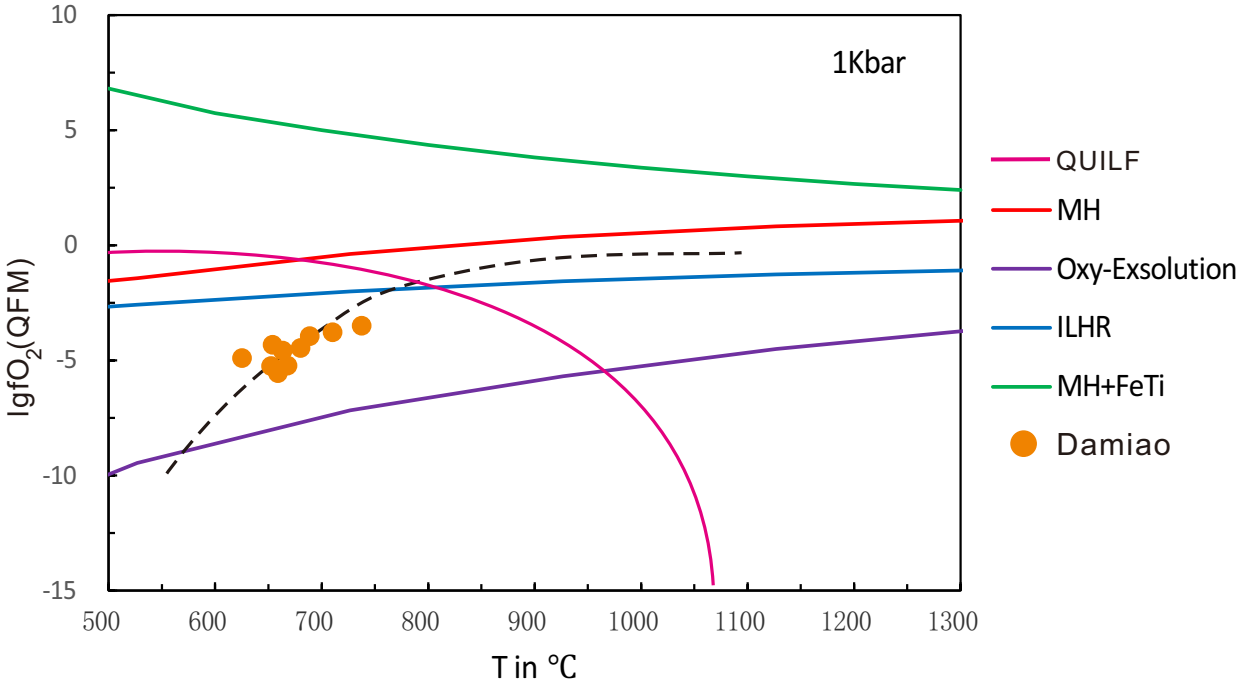
1Kbar
10
5
0
-5
-10
-15
500
600
700
800
900
1000
1100
1200
1300
T in ℃
lgfO2(QFM)
QUILF
MH
Oxy-Exsolution
ILHR
MH+FeTi
Damiao